Published as: *J Mol Biol*. 2009 February 27; 386(3): 869–877.

Aβ(1–40) Fibril Polymorphism Implies Diverse Interaction Patterns in Amyloid Fibrils

Jessica Meinhardt[1,2], **Carsten Sachse**[1,2,6], **Peter Hortschansky**[3], **Nikolaus Grigorieff**[2,4,*], **Marcus Fändrich**[1,5,*]

[1]Leibniz-Institut für Altersforschung (Fritz-Lipmann-Institut), Beutenbergstraße 11, D-07745 Jena, Germany

[2]Brandeis University, MS 029, Waltham, MA 02454-9110, U.S.A.

[3]Leibniz-Institut für Naturstoff-Forschung und Infektionsbiologie (Hans-Knöll-Institut), Beutenbergstraße 11, D-07745 Jena, Germany

[4]Howard Hughes Medical Institute

[5]Max Planck Research Unit for Enzymology of Protein Folding and Martin-Luther University Halle-Wittenberg, Weinbergweg 22, D-06120 Halle (Saale), Germany

[6]Present address: MRC Laboratory of Molecular Biology, Hills Road, Cambridge, CB2 0QH, UK

Abstract

Amyloid fibrils characterize a diverse group of human diseases that includes Alzheimer's disease, Creutzfeldt-Jakob and type II diabetes. Alzheimer's amyloid fibrils consist of Aβ peptide and occur in a range of structurally different fibril morphologies. Using electron cryo-microscopy and three-dimensional reconstruction, we have determined here the structural characteristics of twelve single Aβ(1–40) amyloid fibrils, all formed under the same solution conditions. We find that the majority of analyzed fibrils form a range of morphologies that show almost continuously altering structural properties. The observed fibril polymorphism implies that amyloid formation can lead, for the same polypeptide sequence, to many different patterns of inter- or intra-residue interactions. This property differs significantly from native, monomeric protein folding reactions that produce, for one protein sequence, only one ordered conformation and only one set of inter-residue interactions.

Keywords

amyloid; neurodegeneration; prion; protein folding; structure

INTRODUCTION

Amyloid fibrils are fibrillar polypeptide aggregates that occur inside the human body associated with aging and a group of debilitating diseases, including type II diabetes,

[*]**Corresponding authors**: Marcus Fändrich, Tel: +49 345 5524970; Fax:+49 345 5511972; fandrich@enzyme-halle.mpg.de, or Nikolaus Grigorieff, Tel: +1 781 736 2444; Fax: +1 781 736 2405; niko@brandeis.edu.

Creutzfeldt-Jakob and Alzheimer's disease (AD).[1–3] In the case of AD, amyloid fibrils are formed from amyloid-β (Aβ) peptide.[4] Amyloid fibrils possess a structural spine that is formed by a cross-β structure. This structure consists of oriented β-sheets with strand-strand hydrogen bonds aligned parallel to the main fibril axis. It follows from this arrangement that the amino acid side chains extend perpendicular to the fibril axis and define the intra- or intermolecular interactions within the plane of the fibril cross-section.[2] Therefore, side chain interactions determine several important properties of amyloid fibrils, such as the packing distance between adjacent β-sheets,[5] the regions of self-complementarity of a polypeptide sequence[6,7] and the contact surfaces of juxtaposed protofilaments. Protofilaments represent the filamentous substructures of mature amyloid fibrils[8,9]. Protofilaments are usually twisted, giving rise to the discernible left-handed twist of mature fibrils.[10–12]

Samples of amyloid fibrils commonly exhibit significant structural heterogeneity. Such heterogeneity can arise from variations in bending or twisting of the fibrils, as well as from different fibril morphologies.[13–16] Each fibril morphology is associated with its own specific overall shape, thickness, or twisting.[8–14,16–24] Different fibril morphologies have been attributed to different numbers of protofilaments, [9,11,21,25,26] different protofilament arrangements[12] or different peptide conformations[22,24,27,28]. The conformational specifics of distinct fibril or aggregate morphologies can be propagated by nucleation[29,30] and different aggregate conformations are thought to give rise to different aggregate cytotoxicities[22,31,32] or clinical manifestations in terms of different prion strains[33].

Here, we have determined the diversity of amyloid fibrils formed from Aβ(1–40) peptide *in vitro*. This peptide adopts, within the fibril, a β-sheet conformation.[20,34] Structural models were proposed suggesting that the fibril cross-section encompasses a side-by-side arrangement of either four or eight β-sheet layers.[34] Three-dimensional (3D) reconstruction of one Aβ(1–40) fibril morphology based on electron cryo-microscopy (cryo-EM) data, however, revealed a fibril structure that was different from all previously proposed models.[35,36] Although the 3D-reconstructed fibril also consists of four major β-sheet regions, the latter are arranged into two equal pairs that are offset from each other in the fibril cross-section. However, Aβ(1–40) is known to give rise to different fibril morphologies,[10,11,16,20,22] and the previous cryo-EM analyses could only address the topological characteristics of one specific Aβ fibril morphology. Therefore, we determine here the structural characteristics of different Aβ(1–40) fibril morphologies. The main techniques of our analysis are negative stain transmission electron microscopy (TEM) as well as cryo-EM combined with 3D image reconstruction.

RESULTS

Structural persistence of individual amyloid fibrils.

We found that two parameters are particularly useful for describing different amyloid fibril morphologies: the fibril width (w) and the crossover distance (d). While w corresponds to the lateral fibril extension, crossovers represent apparent constrictions of the fibril width when visualizing the fibrils with TEM techniques (Figure 1(a)). The distance d between two adjacent crossovers equals half the pitch of helically structured fibrils. Analysis of d and w in different amyloid fibrils shows that these values can vary significantly between individual

fibrils (Figure 1(b)). By contrast, *w* and *d* vary only slightly when measured at different positions within the same amyloid fibril (Figure 1(a) and 1B). The high conservation of *w* and *d* at different axial positions of the same fibril implies that the basic structural scaffold is mostly retained along the main axis of a mature fibril. This conclusion is corroborated by comparison of the shape and width of the individual crossovers that occur within the same fibril with those occurring in different fibrils: while a single fibril retains its crossover properties along its main axis, different fibrils can show substantial differences (Figure 2(a)).

Different Aβ amyloid fibrils can show quasi-continuous structural alterations.

Based on measurements of *d* and *w*, we have explored the structural heterogeneity of two samples of Aβ(1–40) fibrils that were obtained by incubation under different conditions. One sample was obtained by incubation of Aβ(1–40) peptide in sodium borate buffer (pH 7.8, 22°C). The other sample was incubated closer to physiologic conditions in phosphate buffered saline (PBS, pH 7.4, 37°C). Judged from their appearance in negative stain (Figure 1(c)), the observed fibril morphologies correspond closely to previously reported Aβ(1–40) fibrils.[11,16,20] Moreover, and consistent with previous reports,[11,16,20] both samples encompass evidently more than one fibril morphology (Figure 1(c)). Even after incubation of the Aβ(1–40) peptide for more than six weeks we did not obtain homogeneous fibril preparations (data not shown). Measurement of 200 randomly selected fibrils from each sample shows that the *w* values can vary from 5 to 26 nm (PBS) or 8 to 23 nm (borate buffer). The *d* values of these fibrils vary between 30 and 330 nm (PBS) or 50 and 380 nm (borate buffer).

A correlation plot of the two properties *d* and *w* produces, for borate fibrils, a cluster of data points that overlaps considerably with the *d/w*-pair distribution of PBS fibrils (Figure 1(d)). Since each *d/w*-pair characterizes a specific fibril structure, the substantial overlap of the two *d/w*-pair distributions implies that most, if not all, borate fibril morphologies occur also in PBS. However, the structural diversity of PBS fibrils is apparently greater than that of borate fibrils. Moreover, 82 % of the PBS fibrils do not allow measurement of a crossover distance. Possible reasons are a higher irregularity of PBS fibrils, their shorter length, and perhaps, a sometimes much lower extent of twisting (Figure 1(c)). Some regions of the *d/w*-plot are populated more densely than others, but it is not possible to unambiguously separate out the measured *d/w* values into clearly distinct subpopulations (Figure 1(d)). Instead, we observe an almost continuous distribution of the measured *d* and *w* values, and of the *d/w*-pairs, suggesting the presence of numerous types of fibrils. This finding is further supported by the 3D reconstructions presented in the next section.

3D reconstruction of twelve single amyloid fibrils by cryo-EM.

We have reconstructed the 3D density of twelve individual amyloid fibrils from one sample (Figure 2(a)); i.e. each of the twelve reconstructions shown in Figure 2(b) was calculated from a single amyloid fibril. All twelve fibrils were grown in borate buffer. Fibrils grown under these conditions were generally found to be longer and better resolved than PBS fibrils (see above). Moreover, borate acts as a negative stain agent,[37] which is an advantage when working with otherwise unstained cryo-EM samples. The only criteria for selecting these 12 fibrils were their relatively straight structure and a length of more than 700 nm.

Otherwise, these fibrils were chosen randomly, without paying attention to their morphologies. The fibrils are numbered according to ascending width, except for fibril 12, which possesses a significantly different structure (see below). Within the series of fibrils 1–11, *w* increases progressively from 10.5 to 21.5 nm (Table 1). Measured *d* values vary from 65 to 163 nm and tend to increase with *w*. Hence, the twelve selected fibrils adequately represent the total *d* and *w* diversity of the fibrils seen in negative stain (Figure 1(c)).

The resolution of the reconstructed densities range from 24 to 39 Å (Table 1, Figure 3) based on the 0.5 Fourier shell correlation criterion. The twelve fibrils show significant crossover periodicity, but no axial 2.7 nm repeat or a tubular substructure.[8,25] Unidirectional platinum shadowing demonstrates that all helical fibrils of this sample possess a left-handed chirality (data not shown). All twelve fibrils were reconstructed twice, once by assuming two-fold rotational symmetry around the fibril axis, and once by assuming no additional symmetry. Two-fold symmetry means that the cross-section superimposes with itself after a 180° rotation. Asymmetry means that this only occurs after a 360° rotation. The pairs of 3D reconstructions obtained for fibrils 1–11 are similar, irrespective of the symmetry assumption used. Therefore, there is good correspondence between the raw data and the projections of the two-fold symmetrical and asymmetrical reconstructions of these fibrils. This is shown in Figure 4(a) and 4(b), using fibril 11 as an example. Hereafter, we only refer to the two-fold symmetrical reconstructions of fibrils 1–11 (see Figure 2(b)). The cross-sectional structures of fibrils 1–11 range from a compact, square-like shape over several cross-sections with relatively elliptical structure to one that is roughly S-shaped (Figure 2(c)). Besides these cross-sectional differences, fibrils 1–11 differ also with respect to the shape and width of their crossovers. For example, fibril 11 possesses crossovers that are prominent and much narrower than the width of this fibril. By contrast, fibril 1 possesses crossovers that are much less pronounced (Figure 2(a)).

While fibrils 1–11 all comply with a two-fold symmetry, fibril 12 does not. Enforcement of a two-fold symmetry on fibril 12 leads to a 3D density map inconsistent with the raw data (Figure 4(c)). Only the asymmetrical reconstruction of this fibril produces a density map that agrees well with the raw data (Figure 4(d)). The fundamental structural difference of fibril 12 compared with the other eleven reconstructed fibrils is also evident from the raw electron micrographs. In these images, the brightest features represent the regions of the highest density in projection (Figure 2(a)). In the case of fibrils 1–11, these regions lie always on the central fibril axis. In the case of fibril 12, however, they are arranged into pairs of two and are offset from the central fibril axis, alternating from the left to the right side (Figure 2(a)). Finally, fibril 12 also shows different mechanical properties compared with the other eleven fibrils, as will be presented in more detail within the next section.

The cross-sectional structure is a determinant of the observable fibril twist.

In the past, the estimation of the fibril cross-section from AFM measurements enabled the calculation of the polar moment of inertia I_z about the main fibril axis *z*.[38] I_z describes the mechanical resistance of a fibril towards torsional stress. In contrast to previous approaches, which estimated I_z values only from the cross-sectional diameter of a fibril,[38] we determine

here the I_z value of each fibril directly from its cross-sectional shape according to the general formula

$$I_z = \int r^2 dA \quad \text{(Equation 1)}$$

where r is the radial distance and A is the cross-sectional area. I_z was originally defined for macroscopic structures that possess homogeneous and isotropic material properties. Although the properties of a fibril on a microscopic and near-atomic scale must be quite different when compared with a macroscopic object, fibrils 1–11 show a clear correlation between I_z and the crossover distance d which describes the twist of a fibril. Within this series, d tends to increase with I_z (Figure 5). A linear fit produces a correlation coefficient R of 0.93. While some two-fold symmetrical fibrils deviate slightly from such a linear relationship, fibril 12 shows more substantial differences. This deviation testifies further to the fundamental structural difference of this fibril.

DISCUSSION

Here we show that Aβ(1–40) peptide can form a range of different amyloid fibril morphologies, even when incubated under the same solution conditions. It is known that different conditions of incubation can lead to different fibril structures. Additionally, this study shows that even within the same sample polymorphic fibril distributions can exist. This observation is consistent with a previous analysis on the effects of salts on Aβ(1–40) fibrils[16] and a study by Goldsbury *et al.*, revealing different types of coiled Aβ(1–40) fibrils and flat ribbons in the same sample.[11] Hence, different incubation conditions produce different polymorphic ensembles of Aβ(1–40) fibril morphologies.

The differences between different Aβ(1–40) fibrils are sometimes rather fundamental, such as in the case of fibril 12, that differs substantially from the other eleven reconstructed fibrils, as shown by its different basic symmetry and different micromechanical properties. However, even two-fold symmetrical fibrils can present significant structural differences, such as fibrils 1, 5 and 11 that differ in properties such as width, crossover distance, cross-sectional structure and in the shape and size of their crossovers (Figure 2(a–c)). Nevertheless, the present study also shows that the differences between different fibrils are sometimes small. These observations are made here by analysis of different Aβ(1–40) samples and by using negative-stain TEM, cryo-EM and 3D reconstruction. For example, Figure 2 shows that fibrils 4, 6, 7 and 8 have an overall similar structure despite some smaller differences. In several samples, the encountered range of fibrils presents almost continuously altering structural properties. This observation is consistent with negative stain TEM analysis of many fibrils from the same sample (Figure 1(d)) as well as with the gallery of 3D fibril reconstructions shown in Figure 2.

We have compared the reconstructed fibrils with previous structural models of Aβ amyloid fibrils. Indeed, fibrils 1 and 11 show clear similarities to some previous models. Fibril 1 possesses a square-shaped cross-section that is compatible with models of a side-by-side arrangement of four major β-sheet regions (Figure 6) as suggested by Petkova *et al.* based on

solid-state nuclear magnetic resonance spectroscopy.[34,39] Fibril 11 is similar to a recently reconstructed Aβ(1–40) fibril[35,36] that represents a double-helix formed from two protofilaments. Each protofilament in this fibril consists of a pair of β-sheet regions, similar to the class 1 steric zipper structures.[6,36] The study by Sachse *et al.* suggests that these β-sheet regions belong to two oppositely directed Aβ peptides, rather than to the previously proposed single Aβ peptide in β-arch conformation[32,34]. Figure 6 shows a corresponding structural arrangement of fibril 11. Given that analysis of this fibril morphology suggests that two β-sheet regions constitute the core of one protofilament,[36] fibrils 1 and 11 may differ mainly in the relative position of two underlying protofilaments. In fibril 1, the two protofilaments are organized side-by-side, while they are offset from one another in fibril 11 (Figure 6).

By contrast, none of the remaining ten single-fibril reconstructions readily corresponds to any previous structural model. Based on proposals that different fibril morphologies can differ in the arrangement of structurally equivalent protofilaments,[9] we have considered this case for fibrils 2–10. Indeed, these fibrils are associated with w and d values and cross-sectional structures in between those of fibrils 1 and 11, consistent with intermediate protofilament-protofilament arrangements. This can be shown also by structural interpretation of fibril 5 (see Figure 6). By contrast, other fibril cross-sections are more difficult to reconcile with such a model. For example, fibril 10 may also involve a different protofilament core structure and peptide-peptide arrangement compared with fibril 11. Such an interpretation is consistent with several reports of peptide microcrystals of zipper-like structures from a seven-residue peptide, which can assume several different modes of packing and conformations.[6,7,40]

The presently described structural heterogeneity of amyloid fibril samples implies that amyloid fibril formation is significantly different from monomeric protein folding reactions. Protein folding reactions are characterized by the fact that a given protein always folds up into the same 3D conformation, irrespective of the pathway through which the native conformation is adopted.[41,42] Hence, all folded molecules share the same inter-residue contacts. By contrast, amyloid formation reactions can lead, for the same polypeptide sequence, to different interresidue contacts. These differences may affect both the contacts within a protofilament as well as those between different protofilaments.

These observations are consistent with concepts according to which amyloid fibril formation represents a generic conformational property of polypeptide chains.[43,44] In other words, the observed amyloid fibril polymorphism reflects the fact that polypeptide chains represent organic polymers and are able to form structural states for which a sequence specificity is much less important than in native protein folding reactions.[5,45] This does not mean that any polypeptide sequence can be arranged in a complementary fashion into an amyloid structure. Analyses by Eisenberg and co-workers have provided evidence that there are actually only a small number of polypeptide chain segments for which this is possible.[46] Compared with native protein folding reactions, however, the side chains possess many different possibilities to interact favorably, so that differently shaped amyloid fibrils arise. These data reconcile the high structural conservation of amyloid fibrils along their main axis, that is, the main-chain dependent cross-β structure, with a high structural diversity, or 'plasticity' of the fibrils,[47]

perpendicular to this direction. Hence, this property of amyloid fibrils resembles chemically much simpler organic polymers, such as polyamide or nylon chains.[48]

Given that the present data shows that Aβ peptide possesses an intrinsic ability to form morphologically heterogeneous amyloid fibrils, we predict that different Aβ amyloid fibril morphologies may also exist inside the human body. Indeed, electron microscopic examination shows that tissue-derived amyloid fibrils formed from apolipoprotein AI, lysozyme and tau protein also possess different morphologies.[18,23] The development of methods to discriminate between these different structures and to manipulate their formation will be important for defining the structural states relevant for conformational diseases. These methods may also enable analysis of how heterogeneous biological activities, such as different prion strains or aggregate cytotoxicities, may be encoded in differently structured aggregates.[49,50]

MATERIAL and METHODS

Fibril preparation.

Amyloid fibrils were grown as described,[51] using final Aβ(1–40) concentrations of 1 mg/ml (with 1 % fibril seeds) and 50 mM sodium borate buffer (pH 7.8) or PBS (pH 7.4). Incubation was carried out for a minimum of two days.

Electron microscopy.

Samples for negative stain analysis were placed on copper grids covered with a carbon film and counterstained with 2 % uranyl acetate, using the droplet technique.[52] Platinum shadowing was carried out as described previously.[35] Specimens were examined in an FEI Morgagni 268 or Zeiss 902 electron microscope operated at an acceleration voltage of 80 kV. Cryo-EM samples were placed onto R 1.2/1.3 holey carbon 400-mesh copper grids (Quantifoil Micro Tools) and plunge-frozen in vitreous ice. Low-dose images of the vitrified specimens were collected at −180°C on a Philips CM12 electron microscope operating at 120 kV. Micrographs were recorded at a nominal magnification of 60,000x and an underfocus of 2.1–2.3 μm on Kodak SO-163 film.

Image processing.

Fibril micrographs were scanned with a raster size of 7 μm, using a Zeiss SCAI flatbed scanner. Averaging of 4 × 4 or 6 × 6 pixels resulted in a final pixel size on the specimen of 0.47 nm or 0.7 nm. A detailed description of the reconstruction procedure can be found elsewhere.[53] Segment sizes were set to either 77 × 77 nm, 112 × 112 nm or 147 × 147 nm (see Table 1). The step size along the fibril axis was 7 nm. Reference projections of fibrils 1 to 11 were computed by rotating about the fibril axis between 0° and 180° in 4° increments and using out-of-plane tilt angles of ± 6.97°, ± 9.83° and ± 12°. This procedure led to a final set of 315 projections. Reference projections of fibril 12 were generated by rotation from 0° to 360°, yielding 630 projections in total. Helical symmetry was imposed with a subunit repeat of 0.47 nm, consistent with X-ray diffraction data.[35] Noise was masked from the obtained 3D models by application of a helical mask. The volumes were low-pass filtered with a cosine falloff to a resolution of 20 Å. At this filter radius, no important structural

details were removed. Fibril reconstructions were displayed with Chimera Visualization System.[54] The thresholds for the representations of fibril surfaces and cross-sections were set so that the fibril widths measured from the raw images and the reconstructions are equal (Table 1).

Calculation of the cross-sectional area and polar moment of inertia.

The cross-sectional areas of the fibril reconstructions were estimated by determination of the number of pixels above the density threshold and converted into square nanometres by multiplication with the pixel size. The values given in Table 1 represent the averages of the cross-sectional areas of the symmetric and asymmetric fibril reconstructions. In the case of fibril 12, only the asymmetric reconstruction was included into the calculation.

The polar moment of inertia I_z was calculated according to equation 1 (see Results), using the dimensions of the reconstructed cross-sections. To simplify computation of I_z, the cross-sectional areas were approximated with one or two rectangles or ellipses.

ACKNOWLEDGMENT

The authors acknowledge technical support from W. Richter (University of Jena, platinum side shadowing). This work was funded through a BioFuture grant (to M.F.) from the Bundesministerium füur Bildung und Forschung (BMBF) as well as through a grant from the Studienstiftung des deutschen Volkes (to J.M.). Currently, C.S. is financially supported by an EMBO long-term postdoctoral fellowship. N.G. gratefully acknowledges financial support from the National Institutes of Health, grant 1 P01 GM-62580.

Abbreviations used:

3D	three-dimensional
Aβ	amyloid-β peptide
AD	Alzheimer’s disease
cryo-EM	electron cryo-microscopy
d	crossover distance
I_z	polar moment of inertia
PBS	phosphate buffered saline
TEM	transmission electron microscopy
w	fibril width

REFERENCES

1. Chiti F & Dobson CM (2006). Protein misfolding, functional amyloid, and human disease. Annu. Rev. Biochem 75, 333–366. [PubMed: 16756495]
2. Fändrich M (2007). On the structural definition of amyloid fibrils and other polypeptide aggregates. Cell. Mol. Life. Sci 64, 2066–2078. [PubMed: 17530168]

3. Westermark P, Benson MD, Buxbaum JN, Cohen AS, Frangione B, Ikeda S, et al. (2005). Amyloid: toward terminology clarification. Report from the Nomenclature Committee of the International Society of Amyloidosis. Amyloid 12, 1–4. [PubMed: 16076605]
4. Finder VH & Glockshuber R (2007). Amyloid-β aggregation. Neurodegener. Dis 4, 13–27. [PubMed: 17429215]
5. Fändrich M & Dobson CM (2002). The behaviour of polyamino acids reveals an inverse side chain effect in amyloid structure formation. EMBO J 21, 5682–5690. [PubMed: 12411486]
6. Sawaya MR, Sambashivan S, Nelson R, Ivanova MI, Sievers SA, Apostol MI, et al. (2007). Atomic structures of amyloid cross-β spines reveal varied steric zippers. Nature 447, 453–457. [PubMed: 17468747]
7. Nelson R, Sawaya MR, Balbirnie M, Madsen AO, Riekel C, Grothe R, et al. (2005). Structure of the cross-β spine of amyloid-like fibrils. Nature 435, 773–778. [PubMed: 15944695]
8. Jimenez JL, Guijarro JI, Orlova E, Zurdo J, Dobson CM, Sunde M, et al. (1999). Cryo-electron microscopy structure of an SH3 amyloid fibril and model of the molecular packing. EMBO J18, 815–821. [PubMed: 10022824]
9. Jimenez JL, Nettleton EJ, Bouchard M, Robinson CV, Dobson CM & Saibil HR (2002). The protofilament structure of insulin amyloid fibrils. Proc. Natl. Acad. Sci. U.S.A 99, 9196–9201. [PubMed: 12093917]
10. Harper JD, Lieber CM & Lansbury PT Jr. (1997). Atomic force microscopic imaging of seeded fibril formation and fibril branching by the Alzheimer's disease amyloid-β protein. Chem. Biol 4, 951–959. [PubMed: 9427660]
11. Goldsbury CS, Wirtz S, Müller SA, Sunderji S, Wicki P, Aebi U, et al. (2000). Studies on the in vitro assembly of Aβ 1–40: implications for the search for Aβ fibril formation inhibitors. J. Struct. Biol 130, 217–231. [PubMed: 10940227]
12. Chamberlain AK, MacPhee CE, Zurdo J, Morozova-Roche LA, Hill HA, Dobson CM, et al. (2000). Ultrastructural organization of amyloid fibrils by atomic force microscopy. Biophys. J79, 3282–3293. [PubMed: 11106631]
13. Abe H & Nakanishi H (2003). Effect of pH on the aggregate formation of a non-amyloid component (1–13). J. Pept. Sci 9, 177–186. [PubMed: 12675500]
14. Bauer HH, Aebi U, Haner M, Hermann R, Müller M & Merkle HP (1995). Architecture and polymorphism of fibrillar supramolecular assemblies produced by in vitro aggregation of human calcitonin. J. Struct. Biol 115, 1–15. [PubMed: 7577226]
15. Knowles TP, Smith JF, Craig A, Dobson CM & Welland ME (2006). Spatial persistence of angular correlations in amyloid fibrils. Phys. Rev. Lett 96, 238301. [PubMed: 16803412]
16. Klement K, Wieligmann K, Meinhardt J, Hortschansky P, Richter W & Fändrich M (2007). Effect of different salt ions on the propensity of aggregation and on the structure of Alzheimer's Aβ(1–40) amyloid fibrils. J. Mol. Biol 373, 1321–1333. [PubMed: 17905305]
17. Goldsbury CS, Cooper GJ, Goldie KN, Müller SA, Saafi EL, Gruijters WTM, et al. (1997). Polymorphic fibrillar assembly of human amylin. J. Struct. Biol 119, 1727.
18. Jimenez JL, Tennent G, Pepys M & Saibil HR (2001). Structural diversity of *ex vivo* amyloid fibrils studied by cryo-electron microscopy. J. Mol. Biol 311, 241–247. [PubMed: 11478857]
19. Bouchard M, Zurdo J, Nettleton EJ, Dobson CM & Robinson CV (2000). Formation of insulin amyloid fibrils followed by FTIR simultaneously with CD and electron microscopy. Protein Sci 9, 1960–1967. [PubMed: 11106169]
20. Malinchik SB, Inouye H, Szumowski KE & Kirschner DA (1998). Structural analysis of Alzheimer's β(1–40) amyloid: protofilament assembly of tubular fibrils. Biophys. J 74, 537–545. [PubMed: 9449354]
21. Ionescu-Zanetti C, Khurana R, Gillespie JR, Petrick JS, Trabachino LC, Minert LJ, et al. (1999). Monitoring the assembly of Ig light-chain amyloid fibrils by atomic force microscopy. Proc. Natl. Acad. Sci. U.S.A 96, 13175–13179. [PubMed: 10557293]
22. Petkova AT, Leapman RD, Guo Z, Yau WM, Mattson MP & Tycko R (2005). Self-propagating, molecular-level polymorphism in Alzheimer's β-amyloid fibrils. Science 307, 262–265. [PubMed: 15653506]

23. Crowther RA & Goedert M (2000). Abnormal tau-containing filaments in neurodegenerative diseases. J. Struct. Biol 130, 271–279. [PubMed: 10940231]
24. Madine J, Jack E, Stockley PG, Radford SE, Serpell LC & Middleton DA (2008). Structural insights into the polymorphism of amyloid-like fibrils formed by region 20–29 of amylin revealed by solid-state NMR and X-ray fiber diffraction. J. Am. Chem. Soc
25. Serpell LC, Sunde M, Benson MD, Tennent GA, Pepys MB & Fraser PE (2000). The protofilament substructure of amyloid fibrils. J. Mol. Biol 300, 1033–1039. [PubMed: 10903851]
26. Goldsbury C, Frey P, Olivieri V, Aebi U & Müller SA (2005). Multiple assembly pathways underlie amyloid-β fibril polymorphisms. J Mol Biol 352, 282–298. [PubMed: 16095615]
27. Verel R, Tomka IT, Bertozzi C, Cadalbert R, Kammerer RA, Steinmetz MO, et al. (2008). Polymorphism in an amyloid-like fibril-forming model peptide. Angew. Chem. Int. Ed. Engl 47, 5842–5845. [PubMed: 18528917]
28. Pedersen JS & Otzen DE (2008). Amyloid-a state in many guises: survival of the fittest fibril fold. Protein Sci 17, 2–10. [PubMed: 18042680]
29. Diaz-Avalos R, King CY, Wall J, Simon M & Caspar DL (2005). Strain-specific morphologies of yeast prion amyloid fibrils. Proc. Natl. Acad. Sci. U.S.A 102, 1016510170.
30. Yamaguchi K, Takahashi S, Kawai T, Naiki H & Goto Y (2005). Seeding-dependent propagation and maturation of amyloid fibril conformation. J. Mol. Biol 352, 952–960. [PubMed: 16126222]
31. Seilheimer B, Bohrmann B, Bondolfi L, Muller F, Stuber D & Döbeli H (1997). The toxicity of the Alzheimer's β-amyloid peptide correlates with a distinct fiber morphology. J. Struct. Biol 119, 59–71. [PubMed: 9216088]
32. Lührs T, Ritter C, Adrian M, Riek-Loher D, Bohrmann B, Döbeli H, et al. (2005). 3D structure of Alzheimer's amyloid-β(1–42) fibrils. Proc. Natl. Acad. Sci. U.S.A 102, 17342–17347. [PubMed: 16293696]
33. Aguzzi A & Haass C (2003). Games played by rogue proteins in prion disorders and Alzheimer's disease. Science 302, 814–818. [PubMed: 14593165]
34. Petkova AT, Ishii Y, Balbach JJ, Antzutkin ON, Leapman RD, Delaglio F, et al. (2002). A structural model for Alzheimer's β-amyloid fibrils based on experimental constraints from solid state NMR. Proc. Natl. Acad. Sci. U.S.A 99, 16742–16747. [PubMed: 12481027]
35. Sachse C, Xu C, Wieligmann K, Diekmann S, Grigorieff N & Fändrich M (2006). Quaternary structure of a mature amyloid fibril from Alzheimer's Aβ(1–40) peptide. J. Mol. Biol 362, 347–354. [PubMed: 16920151]
36. Sachse C, Fändrich M & Grigorieff N (2008). Paired β-sheet structure of an Aβ(1–40) amyloid fibril revealed by electron microscopy. Proc. Natl. Acad. Sci. U.S.A 105, 74627466.
37. Massover WH & Marsh P (1997). Unconventional negative stains: Heavy metals are not required for negative staining. Ultramicroscopy 69, 139–150.
38. Knowles TP, Fitzpatrick AW, Meehan S, Mott HR, Vendruscolo M, Dobson CM, et al. (2007). Role of intermolecular forces in defining material properties of protein nanofibrils. Science 318, 1900–1903. [PubMed: 18096801]
39. Petkova AT, Yau WM & Tycko R (2006). Experimental constraints on quaternary structure in Alzheimer's β-amyloid fibrils. Biochemistry 45, 498–512. [PubMed: 16401079]
40. van der Wel PC, Lewandowski JR & Griffin RG (2007). Solid-state NMR study of amyloid nanocrystals and fibrils formed by the peptide GNNQQNY from yeast prion protein Sup35p. J. Am. Chem. Soc 129, 5117–5130. [PubMed: 17397156]
41. Anfinsen CB (1973). Principles that govern the folding of protein chains. Science 181, 223–230. [PubMed: 4124164]
42. Dobson CM, Sali A & Karplus M (1998). Protein folding: a perspective from theory and experiment. Angew. Chem. Int. Ed 37, 868–893.
43. Chiti F, Webster P, Taddei N, Clark A, Stefani M, Ramponi G, et al. (1999). Designing conditions for in vitro formation of amyloid protofilaments and fibrils. Proc. Natl. Acad. Sci. U.S.A 96, 3590–3594. [PubMed: 10097081]
44. Fändrich M, Fletcher MA & Dobson CM (2001). Amyloid fibrils from muscle myoglobin. Nature 410, 165–166. [PubMed: 11242064]

45. Krebs MR, Macphee CE, Miller AF, Dunlop IE, Dobson CM & Donald AM (2004). The formation of spherulites by amyloid fibrils of bovine insulin. Proc. Natl. Acad. Sci. U.S.A 101, 14420–14424. [PubMed: 15381766]

46. Thompson MJ, Sievers SA, Karanicolas J, Ivanova MI, Baker D & Eisenberg D (2006). The 3D profile method for identifying fibril-forming segments of proteins. Proc. Natl. Acad. Sci. U.S.A 103, 4074–4078. [PubMed: 16537487]

47. Wetzel R, Shivaprasad S & Williams AD (2007). Plasticity of amyloid fibrils. Biochemistry 46, 1–10. [PubMed: 17198370]

48. Bunn CW & Garner EV (1947). The crystal structure of two polyamides ('nylons'). Proc. R. Soc. Lond. Ser. A 189, 39–68.

49. Prusiner SB (1998). Prions. Proc. Natl. Acad. Sci. U.S.A 95, 13363–13383. [PubMed: 9811807]

50. Caughey B & Lansbury PT Jr. (2003). Protofibrils, pores, fibrils, and neurodegeneration: separating the responsible protein aggregates from the innocent bystanders. Annu. Rev. Neurosci 26, 267–298. [PubMed: 12704221]

51. Peim A, Hortschansky P, Christopeit T, Schroeckh V, Richter W & Fandrich M(2006). Mutagenic exploration of the cross-seeding and fibrillation propensity of Alzheimer's β-amyloid peptide variants. Protein Sci 15, 1801–1805. [PubMed: 16751608]

52. Harris JR (1997). Negative Staining and Cryoelectron Microscopy: the thin film techniques, Bios Scientific Publishers, Oxford, UK.

53. Sachse C, Chen JZ, Coureux PD, Stroupe ME, Fandrich M & Grigorieff N (2007). High-resolution electron microscopy of helical specimens: a fresh look at tobacco mosaic virus. J. Mol. Biol 371, 812–835. [PubMed: 17585939]

54. Pettersen EF, Goddard TD, Huang CC, Couch GS, Greenblatt DM, Meng EC, et al. (2004). UCSF Chimera - a visualization system for exploratory research and analysis. J. Comput. Chem 25, 1605–1612. [PubMed: 15264254]

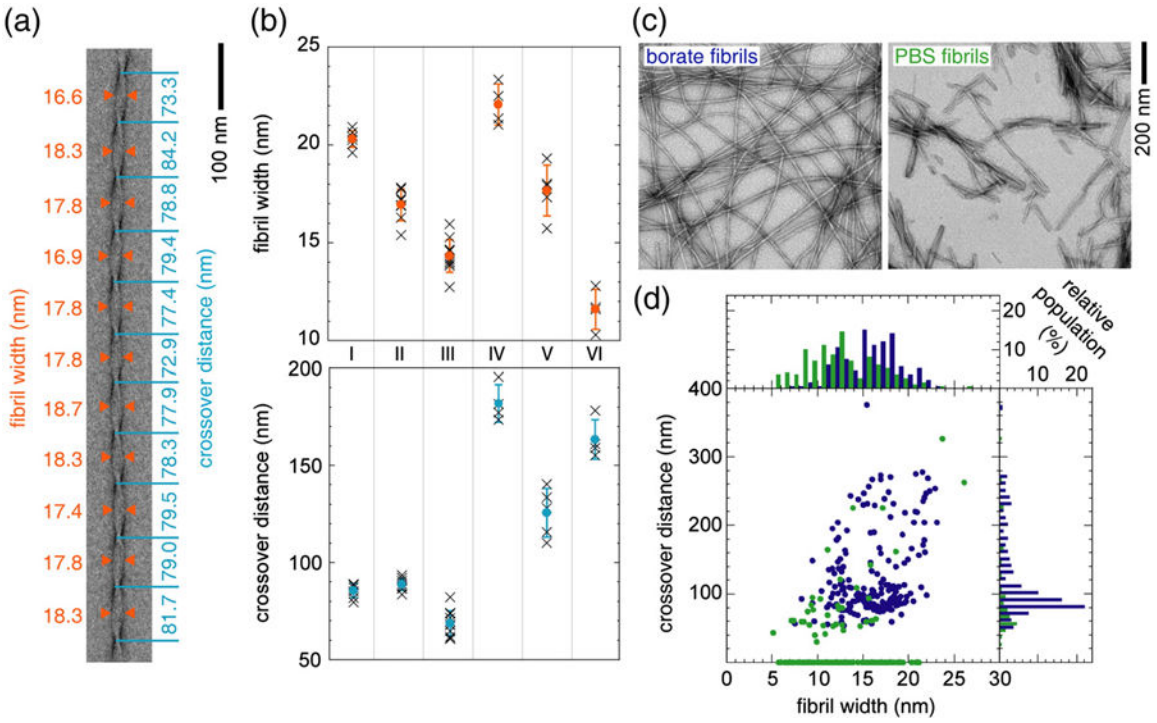

Figure 1.

Demonstration of the structural persistence and morphological diversity of Aβ(1–40) fibrils. (a) Example measurement of fibril width and crossover distance at different positions of the same fibril. (b) Plot of fibril width and crossover distance measured for six different fibrils grown in 50 mM borate (pH 7.8) at 22°C. Each column I to VI shows the values measured at different positions of the same fibril (crosses) and their mean with standard deviation (filled circles). (c) Negative staining images of Aβ (1–40) fibrils grown either in 50 mM borate (pH 7.8) at 22°C or in PBS (pH 7.4) at 37°C. (d) Distribution of fibril width (w) and crossover distance (d) of different individual fibrils formed in borate buffer (black) or PBS (gray). Data points with $d=0$ represent fibrils with no measurable d value (see text for details).

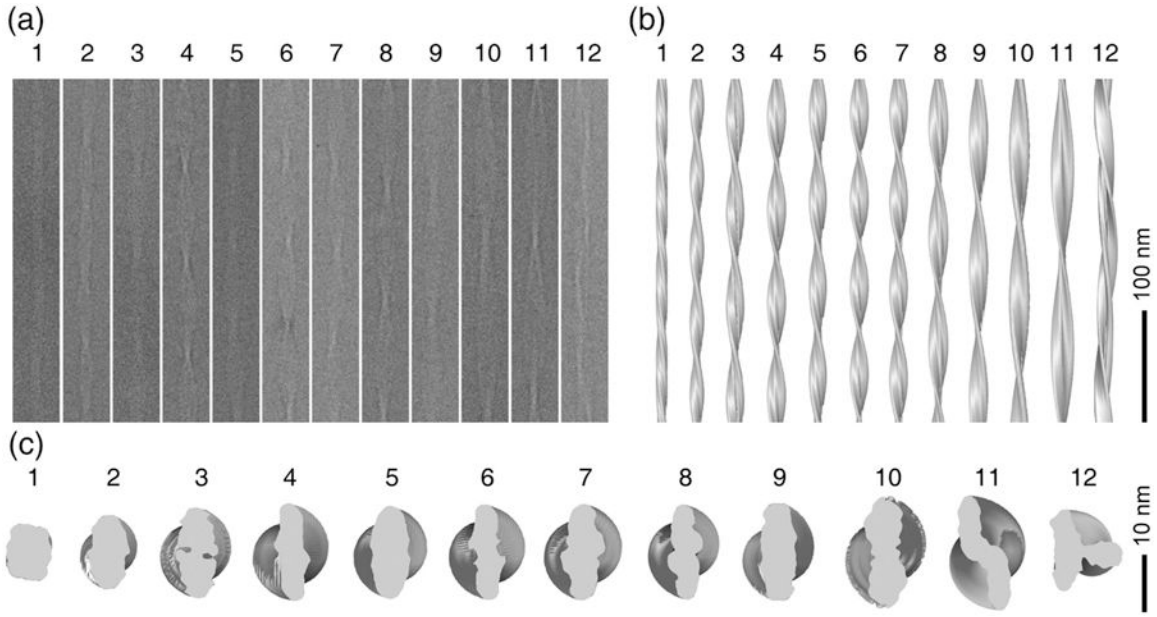

Figure 2.

Cryo-EM reconstructions of twelve individual Aβ(1–40) fibrils. (a) Electron micrographs of the twelve individual Aβ(1–40) fibrils from the same sample. (b, c) Side (b) and top (c) views of the reconstructed fibrils shown in (a).

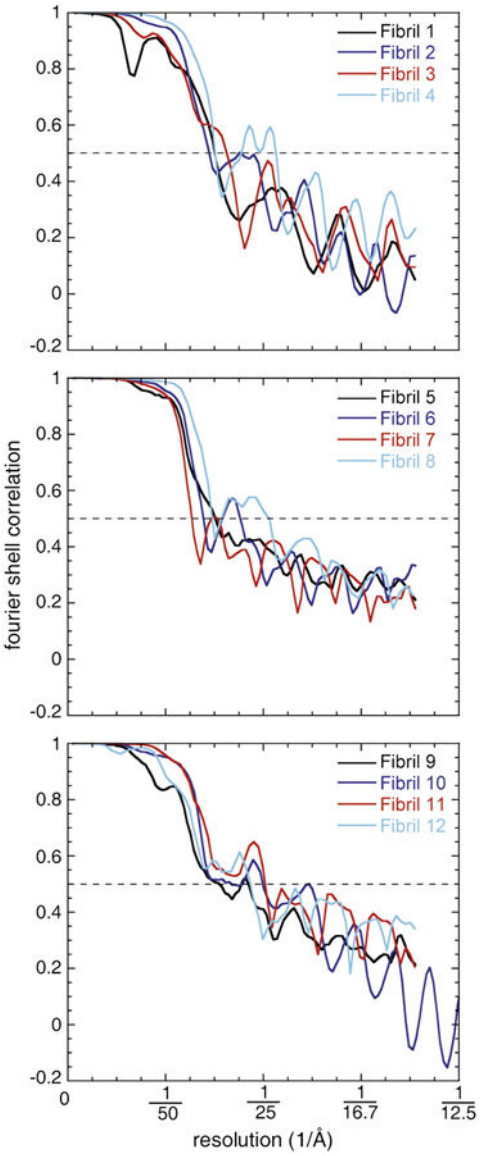

Figure 3.

Resolution assessment using the Fourier shell correlation curve. The Fourier shell correlation curves of the fibril reconstructions indicate the following resolutions at the 0.5 cut-off criterion (dashed line): fibril 1: 33 Å, fibril 2: 34 Å, fibril 3: 30 Å, fibril 4: 33 Å, fibril 5: 33 Å, fibril 6: 36 Å, fibril 7: 39 Å, fibril 8: 33 Å, fibril 9: 32 Å, fibril 10: 30 Å, fibril 11: 24 Å, fibril 12: 26 Å. The curves show several minima that occur at spatial frequencies with poor signal owing to the characteristics of the contrast transfer function of the electron microscope.

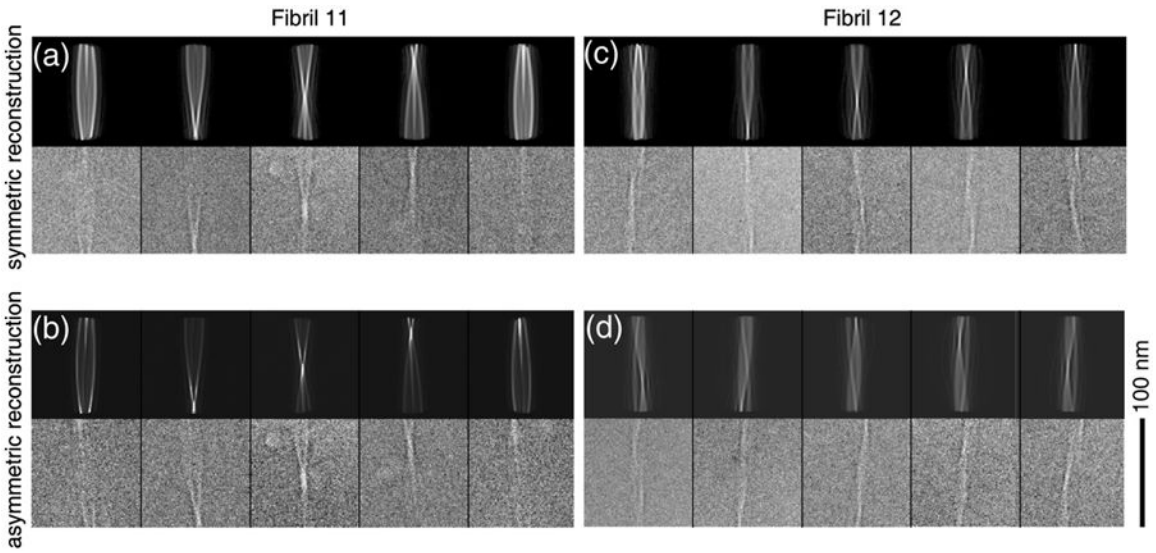

Figure 4.

Comparison of the reconstructed densities with the raw data at different axial rotation angles. (a, b) Projections of both the two-fold symmetrical reconstruction (a) and asymmetrical reconstruction (b) of fibril 11 agree well with the raw images. (c) The two-fold symmetric reconstruction of fibril 12 does not show a good match with the original data. (d) Reconstruction of fibril 12 without this symmetry assumption produces a good agreement with the raw data. In all panels: upper row - projections of the reconstruction; bottom row - raw data.

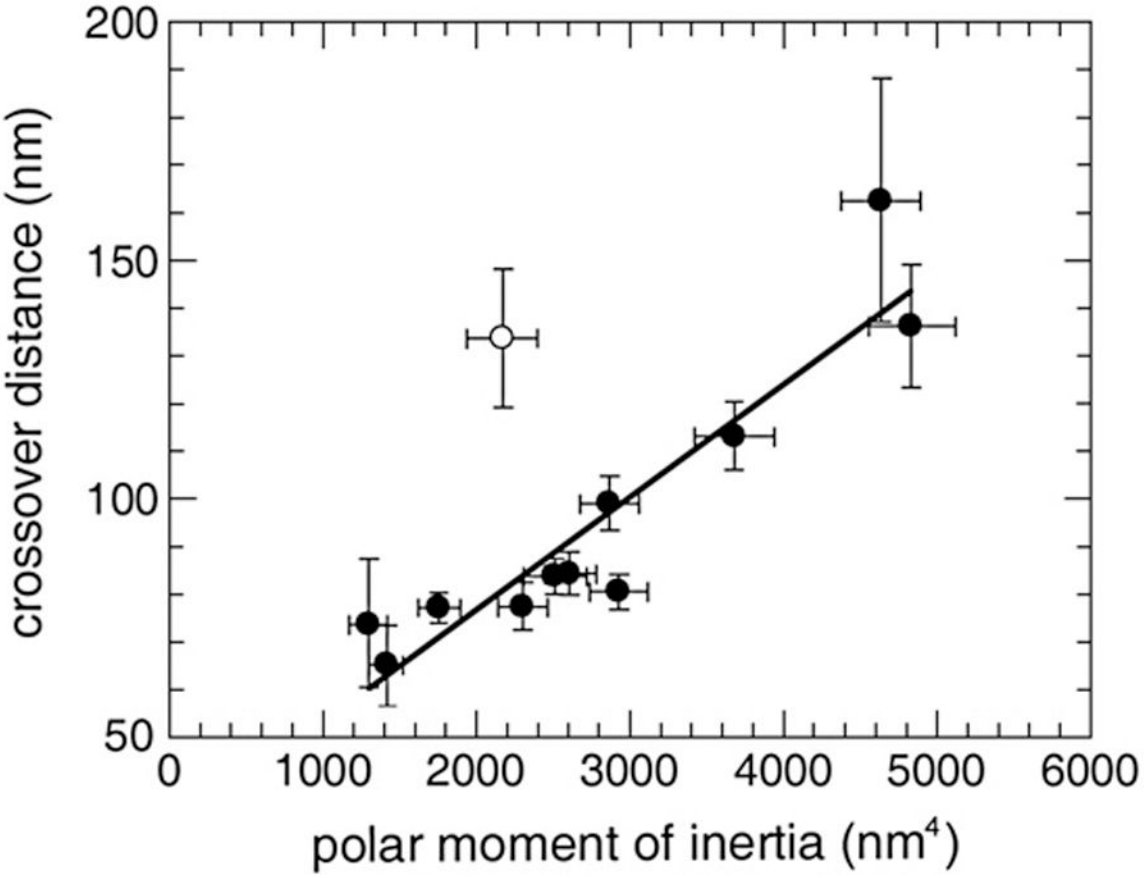

Figure 5.
Correlation between crossover distance (*d*) and polar moment of inertia (I_z). Data taken from Table 1. Filled circles represent fibrils 1–11, open circle represents fibril 12. Only the data points of fibrils 1–11 are fitted with a straight line (R = 0.93).

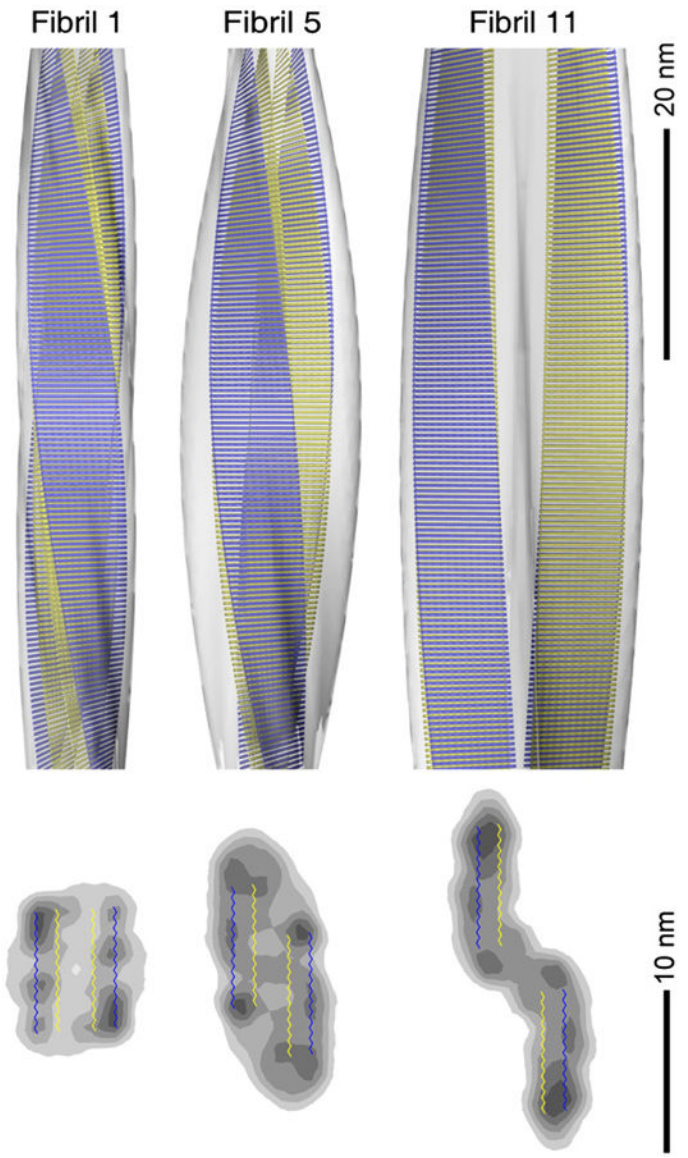

Figure 6.

Structural model of the protofilament core topology of fibrils 1, 5 and 11. Top: side view of the fibrils with two protofilament cores modelled into the densities. Bottom: contoured density cross-sections of the fibrils superimposed with two protofilament cores. Each protofilament core comprises a pair of two β-sheet regions colored in yellow (interface) and blue (outside). Each β-sheet region may be formed by one Aβ peptide as suggested by a recent analysis of a morphology corresponding to fibril 11.[36] To date, it is not known whether a β-sheet region consists of a single long strand or whether it is constructed from several short β-sheet segments.

Table 1.

Properties of the twelve reconstructed fibrils and reconstruction details.

Fibril	*w* (nm)	*d* (nm)	Segment size (nm)	Segment number	Resolution (Å)	Cross-sectional area (nm^2)	I_z (nm^4)
1	10.5 ± 1.2	74 ± 13	112	59	33	67 ± 13	1298±111
2	13.6 ± 1.6	65 ± 8	112	65	34	75 ± 15	1419±104
3	16.5 ± 2.1	84 ± 4	112	84	30	77 ± 15	2606 ±166
4	16.9 ± 1.3	84 ± 3	147	114	33	74 ± 15	2509 ± 203
5	17.4 ± 1.5	77 ± 5	147	152	33	93 ± 19	2303 ± 152
6	17.7 ± 1.1	77 ± 3	147	90	36	72 ± 14	1757±130
7	17.8 ± 1.5	80 ± 3	147	140	39	90 ± 18	2927±181
8	18.3 ± 1.5	99 ± 5	77	158	33	76 ± 15	2868 ±182
9	19.1 ± 1.4	113 ± 7	147	109	32	92 ± 18	3680 ± 252
10	20.3 ± 1.4	136 ± 13	147	213	30	103 ± 21	4831± 279
11	21.5 ± 1.6	163 ± 25	112	121	24	88 ± 18	4634 ± 248
12	12.1 ± 1.7	134 ± 14	112	142	26	91± 18	2172 ± 218

Fibril width *w* and the crossover distance *d* represent averages from a minimum of eight single measurements and are given with their standard deviations. An error of 20 % was assumed for the cross-sectional areas, based on the errors of *w* that are typically about 10 %. Errors on I_Z were estimated from the measurement uncertainty of the dimensions of the fibril cross-section.